



HAL
open science

Synthesis of $\text{La}_{9.33}\text{Si}_6\text{O}_{26}$ Pore–Solid Nanoarchitectures via Epoxide-Driven Sol–Gel Chemistry

Stephane Celerier, Christel Laberty, J. W. Long, K. A. Pettigrew, Rhonda M. Stroud, D.R. Rolison, Florence Ansart, Philippe Stevens

► **To cite this version:**

Stephane Celerier, Christel Laberty, J. W. Long, K. A. Pettigrew, Rhonda M. Stroud, et al.. Synthesis of $\text{La}_{9.33}\text{Si}_6\text{O}_{26}$ Pore–Solid Nanoarchitectures via Epoxide-Driven Sol–Gel Chemistry. *Advanced Materials*, 2006, 18 (5), pp.615-618. 10.1002/adma.200501938 . hal-02183999

HAL Id: hal-02183999

<https://hal.science/hal-02183999>

Submitted on 7 Nov 2023

HAL is a multi-disciplinary open access archive for the deposit and dissemination of scientific research documents, whether they are published or not. The documents may come from teaching and research institutions in France or abroad, or from public or private research centers.

L'archive ouverte pluridisciplinaire **HAL**, est destinée au dépôt et à la diffusion de documents scientifiques de niveau recherche, publiés ou non, émanant des établissements d'enseignement et de recherche français ou étrangers, des laboratoires publics ou privés.

Synthesis of $\text{La}_{9.33}\text{Si}_6\text{O}_{26}$ Pore–Solid Nanoarchitectures via Epoxide-Driven Sol–Gel Chemistry**

By *Stephane Célérier, Christel Laberty-Robert,* Jeffrey W. Long, Katherine A. Pettigrew, Rhonda M. Stroud, Debra R. Rolison, Florence Ansart, and Philippe Stevens*

Silicate-based oxides are of interest as electrolytes and electrode materials in intermediate-temperature solid-oxide fuel cells (SOFCs).^[1–7] We have developed a sol–gel-based strategy for the production of mesoporous, nanostructured, single-phase $\text{La}_{9.33}\text{Si}_6\text{O}_{26}$ apatite in an aerogel-type framework. Silicon alkoxides react with lanthanum(III) aqueous ions in alcohol solutions driven by a proton-scavenging agent, propylene oxide. Varying the means by which pore fluid is removed from the resultant lanthanum silicate gels yields three distinct pore–solid monolithic nanoarchitectures: aerogels, ambigels, and xerogels. The ambigel and aerogel nanoarchitectures exhibit high specific surface areas (from 285 to 408 m^2g^{-1}), aperiodic through-connected networks of mesopores, and covalently bonded networks of non-agglomerated nanoparticles. Calcination at relatively mild temperatures for this oxide (800 °C) converts the amorphous gels to nanocrystalline apatite $\text{La}_{9.33}\text{Si}_6\text{O}_{26}$. Although densified during calcination, the aerogel and ambigel nanoarchitectures retain porosity, high surface area, and limited particle agglomeration.

Aerogels and related highly porous architectures are defined by a bonded three-dimensional network of nanoparticles, commingled with interconnected porosity.^[8–10] The inherent structural characteristics of aerogels are highly beneficial for electrochemical applications,^[9] where the high interfacial surface area enhances the kinetics of electrochemical reactions and the continuous mesoporous network facilitates the transport of molecules, ions, and nanoscale objects to the active electrode surface while the solid network of covalently linked nanoparticles promotes charge transport of electrons

and ions. It is only recently that aerogel-like materials have been synthesized in electrically conductive, SOFC-relevant compositions and then characterized at operating temperatures.^[11,12]

An earlier sol–gel route to mixed La–Si oxides modified an acid-catalyzed silica sol–gel method by including lanthanum salts.^[13,14] Investigation of a range of hydrolysis rates showed that only very narrow synthesis conditions led to apatite $\text{La}_{9.33}\text{Si}_6\text{O}_{26}$ upon calcination (800 °C),^[1] and impurity phases were common. Subsequent attempts to produce aerogels or ambigels (requiring washing steps with ethanol) led to amorphous oxides after calcination (1000 °C), suggesting that this protocol generates a silica network with the lanthanum salt dispersed on its surface.^[1]

Our approach to synthesize lanthanum silicate nanoarchitectures is based on the initial formation of oligomers of La–O–Si by using epoxide- and alkoxide-driven hydrolysis and condensation reactions. This synthetic protocol is a modification of innovative methods reported by Gash et al. for the preparation of transition metal oxide aerogels.^[15–17] This route was recently extended to mixed transition metal oxide aerogels^[11,18] and nanocomposites of silica and metal oxide.^[19,20] We obtain gels by mixing tetramethoxysilane (TMOS) into methanolic solutions of $\text{LaCl}_3 \cdot 6\text{H}_2\text{O}$ and then adding propylene oxide; the gels are processed as described in the Experimental section to form three different pore-solid nanoarchitectures.

The lanthanum silicate aerogels and ambigels are transparent and monolithic (Fig. 1a), similar to base-catalyzed silica aerogels, and exhibit the amorphous, pearl-necklace structure characteristic of silica (Fig. 1b). The aerogel retains the low-density structure of the wet gels (0.07 g cm^{-3}), whereas the ambigel suffers obvious shrinkage (see Fig. 1a) in keeping with an envelope density of 0.21 g cm^{-3} .

The pore structure of the various $\text{La}_{9.33}\text{Si}_6\text{O}_x$ nanoarchitectures is assessed via N_2 -physisorption analysis (Table 1). The aerogel and ambigel nanoarchitectures exhibit type-4 isotherms with H3-type hysteresis loops (not shown), indicative of an interconnected mesoporous system.^[21] Pore-size distribution plots, derived from the N_2 -adsorption isotherms, show a range of pores extending from the mesoporous to the macroporous regime (Fig. 2). The aerogels exhibit the highest pore volume (3.07 cm^3g^{-1}), which is distributed around the volume-weighted peak at 50 nm. The ambigels have a considerably narrowed size distribution, with the volume-weighted peak at 10–20 nm. In contrast, the xerogels present type-2 iso-

[*] Prof. C. Laberty-Robert, Dr. J. W. Long, Dr. K. A. Pettigrew, Dr. R. M. Stroud, Dr. D. R. Rolison
U.S. Naval Research Laboratory
4555 Overlook Avenue SW, Washington, DC 20375 (USA)
E-mail: christel.laberty@nrl.navy.mil

S. Célérier, Prof. C. Laberty-Robert, Prof. F. Ansart
UMR5085-CNRS, Université Paul Sabatier, Bât II R1
F-31062 Toulouse Cedex 04 (France)

Dr. P. Stevens
EDF R&D/ElFER
Emmy-Noether-Str. 11, D-76131 Karlsruhe (Germany)

[**] This work was supported in part by the U.S. Office of Naval Research. S. C. received an education training grant from the Université de Toulouse, EDF, and ADEME; K. A. P. is an NRC-NRL Postdoctoral Associate (2004–2007).

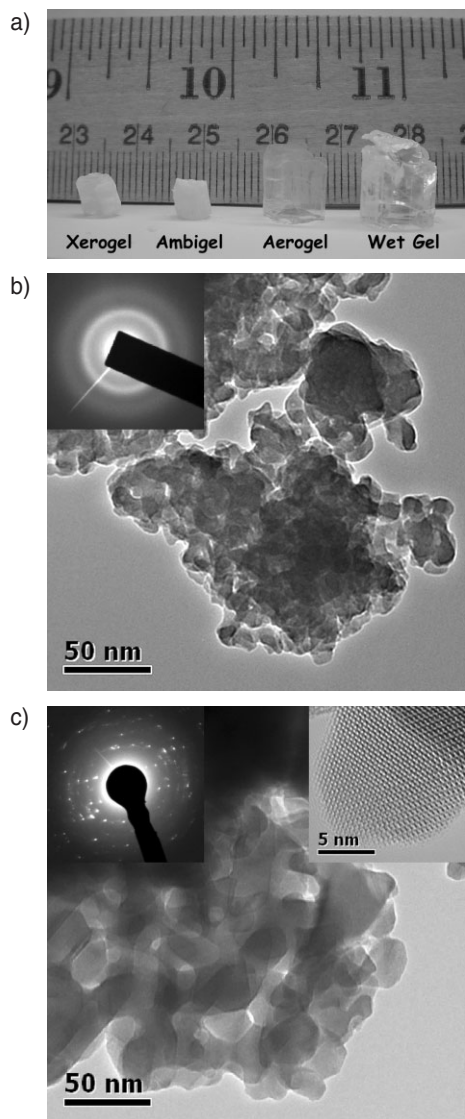


Figure 1. a) Wet lanthanum silicate gel (far right) contrasted with $\text{La}_{9.33}\text{Si}_6\text{O}_x$ aerogel, ambigel, and xerogel. High-resolution transmission electron microscopy images of b) as-prepared and c) calcined (800°C) $\text{La}_{9.33}\text{Si}_6\text{O}_x$ ambigels with corresponding electron diffraction patterns.

Table 1. Surface area and porosity data for $\text{La}_{9.33}\text{Si}_6\text{O}_x$ nanoarchitectures. BET: Brunauer–Emmett–Teller; BJH: Barrett–Joyner–Halenda.

$\text{La}_{9.33}\text{Si}_6\text{O}_x$ nanoarchitectures	Calcination temperature [$^\circ\text{C}$]	BET surface area [m^2g^{-1}]	BJH cumulative pore volume [cm^3g^{-1}]
Aerogel	as-prepared	408	3.07
Aerogel	800	44	0.09
Aerogel	1000	32	0.07
Ambigel	as-prepared	265	0.63
Ambigel	800	34	0.35
Ambigel	1000	18	0.04
Xerogel	as-prepared	312	0.18
Xerogel	800	12	0.05
Xerogel	1000	10	0.06

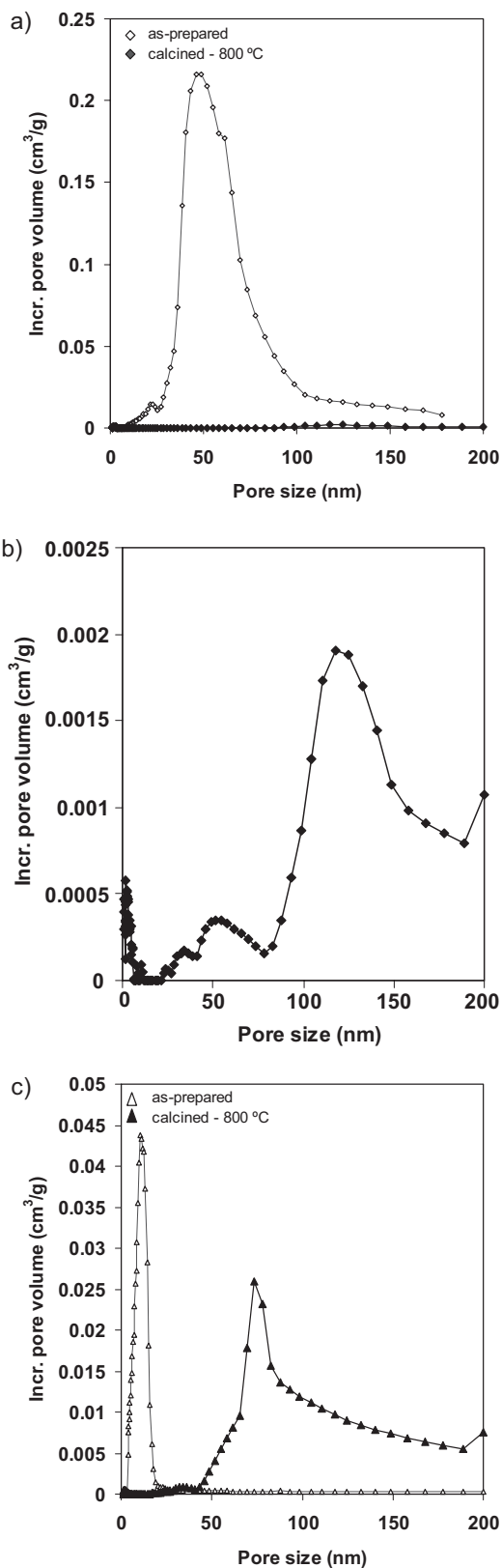


Figure 2. Pore-size distribution plots for aerogels of $\text{La}_{9.33}\text{Si}_6\text{O}_{26}$ a) as prepared and b) after calcination at 800°C ; and c) ambigels of $\text{La}_{9.33}\text{Si}_6\text{O}_{26}$ as-prepared and after calcination at 800°C .

therms, consistent with micropores (<2 nm). The specific surface areas achieved for the as-synthesized $\text{La}_{9.33}\text{Si}_6\text{O}_x$ aerogel ($408 \text{ m}^2 \text{ g}^{-1}$) and ambigel ($265 \text{ m}^2 \text{ g}^{-1}$) are comparable to those obtained for many oxide-based aerogels.^[22]

As most of the applications of lanthanum silicates require high-temperature operation ($\approx 800 \text{ }^\circ\text{C}$), we examined the effects of various thermal treatments on the amorphous as-synthesized nanoarchitectures. The lanthanum silicate gels crystallize to a single phase upon heating at $800 \text{ }^\circ\text{C}$, as evidenced by electron (Fig. 1c) and X-ray (Fig. 3) diffraction analyses; the d -spacings match those of the $\text{La}_{9.33}\text{Si}_6\text{O}_{26}$ apatite structure.^[23,24] The crystallization temperature is quite low when compared to single-phase $\text{La}_{9.33}\text{Si}_6\text{O}_{26}$ prepared by a solid-state method ($1500 \text{ }^\circ\text{C}$),^[5] thus preventing detrimental particle growth, which is advantageous for the projected applications of these materials.

Transforming the amorphous nanoarchitecture into nanocrystalline $\text{La}_{9.33}\text{Si}_6\text{O}_{26}$ is accompanied by decreased surface area and pore volume, rearranged pore-size distribution, and particle growth. However, the ambigel and aerogel still exhibit type-4 isotherms, confirming that the interconnected, open nature of the mesoporous network is conserved, which is beneficial for transporting gaseous reactants and products in SOFC electrode structures. Even when calcined at $1000 \text{ }^\circ\text{C}$ for 10 h, the $\text{La}_{9.33}\text{Si}_6\text{O}_{26}$ aerogels and ambigels retain high specific surface areas (Table 1). Calcining the aerogel nanoarchitectures at $800 \text{ }^\circ\text{C}$ sharply decreases the cumulative pore volume from 3.07 to $0.09 \text{ cm}^3 \text{ g}^{-1}$. The more rugged ambigel does not exhibit such a large loss, decreasing from 0.63 to $0.35 \text{ cm}^3 \text{ g}^{-1}$, but its pore-size distribution is significantly broadened and the peak pore-size shifts to 75 nm (see Fig. 2). Calcining ambigels to $1000 \text{ }^\circ\text{C}$ does not markedly increase densification (see Table 1).

The calcined nanoarchitectures exhibit well-defined particles with edges and steps (Fig. 1c); ambigels calcined to

$800 \text{ }^\circ\text{C}$ have $10\text{--}12 \text{ nm}$ $\text{La}_{9.33}\text{Si}_6\text{O}_{26}$ crystallites that grow to $20\text{--}30 \text{ nm}$ after calcination at $1000 \text{ }^\circ\text{C}$. Even 30 nm crystallites are relatively small compared to $\text{La}_{9.33}\text{Si}_6\text{O}_{26}$ prepared by other methods,^[5] which is expected because the networked solid of the aerogel and ambigel inhibits particle growth.^[25]

Obtaining single-phase $\text{La}_{9.33}\text{Si}_6\text{O}_{26}$ using sol-gel chemistry, rather than a silica/lanthanum oxide nanocomposite, is important for the use of this class of silicates in SOFC electrolytes. Because we were unable to create gels by adding either TMOS to methanolic solutions of $\text{LaCl}_3 \cdot 6\text{H}_2\text{O}$ or epoxide to methanolic solutions of TMOS, we posit that La-O-Si oligomers form, which upon gelation create a mixed La-Si oxide network. Infrared spectroscopy supports the presence of the La-O-Si functionality because the asymmetric Si-O-Si stretch shifts from 1085 cm^{-1} in the as-prepared silica aerogel to $\sim 985 \text{ cm}^{-1}$ in the as-prepared $\text{La}_{9.33}\text{Si}_6\text{O}_x$ aerogel. Prior IR investigations of mixed-metal oxides based on silica have shown that the Si-O-Si stretch (at $\sim 1085 \text{ cm}^{-1}$) red-shifts upon incorporation of other metals (such as nickel and cobalt) to form Si-O-M moieties.^[26]

We propose a three-stage mechanism leading to the formation of lanthanum silicate gels: i) epoxide-promoted hydrolysis^[15] to form $\text{La}(\text{OH})_x(\text{H}_2\text{O})_y^{(3-x)+}$; ii) nucleophilic attack by $\text{La}(\text{OH})_x(\text{H}_2\text{O})_y^{(3-x)+}$ on Si-OR bonds to form La-O-Si oligomers; and iii) polycondensation of the La-O-Si oligomers.

Our sol-gel protocol can be readily adapted to prepare composite materials or additional mixed metal oxides with complex formulations. Adding $\text{SrCl}_3 \cdot 6\text{H}_2\text{O}$ during the synthesis of the lanthanum silicate sol yields a homogeneous oxide gel that contains lanthanum, strontium, and silicon. The synthesis of pure $\text{La}_{9.33-x}\text{Sr}_x\text{Si}_6\text{O}_{26+y}$ is beneficial for SOFC application because its ionic conductivity ($1.9 \times 10^{-2} \text{ S cm}^{-1}$ at $800 \text{ }^\circ\text{C}$ for $\text{La}_9\text{SrSi}_6\text{O}_{26.5}$ ^[27]) is higher than that of the undoped material ($2.9 \times 10^{-3} \text{ S cm}^{-1}$ ^[28]). By adding colloidal solids to an about-to-gel^[29-31] lanthanum silica sol, composite

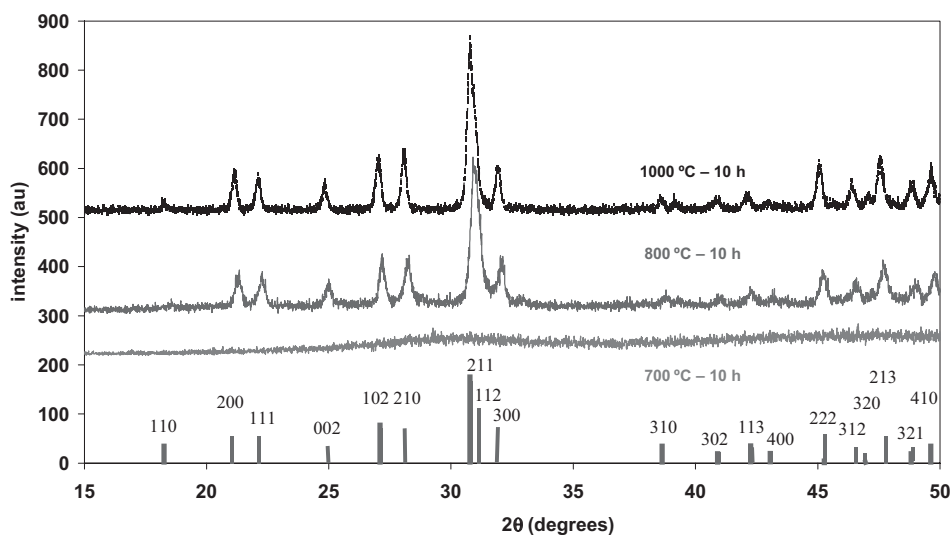


Figure 3. X-ray diffraction of $\text{La}_{9.33}\text{Si}_6\text{O}_{26}$ ambigel calcined at various temperatures ($1000 \text{ }^\circ\text{C}$, $800 \text{ }^\circ\text{C}$, $700 \text{ }^\circ\text{C}$) referenced to the JCPDF (76-0340) file for bulk $\text{La}_{9.33}\text{Si}_6\text{O}_{26}$.

nanoarchitectures are formed that retain the properties of each component. By analogy with our previous studies on room-temperature oxidation of carbon monoxide over Au–TiO₂ aerogels,^[31] we expect that similar composite structures composed of nickel metal nanoparticles and lanthanum silicate aerogels will contain optimized three-phase boundary catalytic sites for use as SOFC anodes.

We can also prepare dense (90–95 %) ceramics by calcining lanthanum silicate ambigel powders at 1400 °C. By contrast, calcining the lanthanum silicate xerogel powder at 1400 °C yields densities of 70–80 %, and a temperature of 1700 °C is required to achieve densities of 90–95 % using solid–solid powder synthesis.^[32] Our present efforts are devoted to preparing these materials as thick films and evaluating their potential for SOFC and sensor applications.

In summary, we describe a low-temperature, facile route to synthesize single-phase complex silicates as porous nanocrystalline apatites. The fluid-filled, sol–gel-derived materials can be dried to form nanoarchitectures with high surface areas and through-connected porosity; this morphology permits sintering to dense ceramics at lower temperatures relative to other nanocrystalline forms. The epoxide-driven sol–gel chemistry is readily adapted to multicomponent silicates containing rare-earth elements as well as second-phase nanoparticles of relevance to catalytic reactions.

Experimental

Materials Synthesis: LaCl₃·6H₂O was dissolved in methanol; TMOS in a La/Si atomic ratio of 1.55 was added; this mixture was stirred for ~10 min and propylene oxide was added. The reaction mixture was poured into polypropylene molds and covered, and the resultant gels were aged for 24 h. The aged gels were solvent-exchanged in 200 proof ethanol for 3–5 days, with the solvent changed twice daily, and acetone-washed twice daily over 4–5 days.

For the preparation of xerogels, excess acetone was decanted and the gel dried at 60 °C under a nitrogen flow for 2 days. For the preparation of ambigels, the acetone pore fluid was exchanged with cyclohexane daily over 4–5 days and then dried at 20–60 °C under a nitrogen flow for 2 days. For the preparation of aerogels, the acetone-filled gels were transferred into a critical-point dryer (Polaron Range, Quorum Technologies, New Haven, East Sussex, UK) and maintained at 10 °C. After a series of exchanges with liquid CO₂ over 6 h, the temperature was increased to 40 °C (critical temperature T_c = 31 °C; critical pressure P_c = 7.44 MPa). The autoclave was slowly vented.

Measurements: All samples were degassed at 150 °C for at least 24 h prior to nitrogen-physisorption measurements (Micromeritics ASAP 2010 Accelerated Surface Area and Porosimetry Analyzer). Pore-size distributions were calculated from adsorption isotherm data using Micromeritics DFTPlusR software (Halsey Thickness model, cylindrical pore). For transmission electron microscopy (JEOL 2010F TEM equipped with a Gatan charge-coupled device camera), samples were ground and then brushed onto holey-carbon film supports. Prior to infrared spectroscopy analysis (IR-10110, Madison Instruments Inc.), each sample was diluted in IR-grade potassium bromide (2 wt.-% as-prepared aerogel) and pressed at ≤ 1500 lb in⁻² (1 lb in⁻² ~ 6.894 kPa) into self-supported discs (13 mm in diameter). Spectra were collected under N₂ with 25 scans at a resolution of 0.5 cm⁻¹ and

referenced to background spectra collected under the same conditions.

- [1] S. Célérier, C. Laberty, F. Ansart, P. Lenormand, P. Stevens, *Ceram. Int.* **2006**, *32*, 271.
- [2] S. Nakayama, T. Kageyama, H. Aono, Y. Sadaoka, *J. Mater. Chem.* **1995**, *5*, 1801.
- [3] S. Nakayama, M. Sakamoto, *J. Eur. Ceram. Soc.* **1998**, *18*, 1413.
- [4] E. J. Abram, D. C. Sinclair, A. R. West, *J. Mater. Chem.* **2001**, *11*, 1978.
- [5] S. Nakayama, M. Higuchi, *J. Mater. Sci. Lett.* **2001**, *20*, 913.
- [6] J. McFarlane, S. Barth, M. Swaffer, J. E. H. Sansom, P. R. Slater, *Ionics* **2002**, *8*, 149.
- [7] S. Beaudet Savignat, A. Lima, C. Barthet, A. Henry, in *Electrochem. Soc. Proc. PV2003-07*, The Electrochemical Society, Pennington, NJ **2003**, p. 372.
- [8] J. Fricke, A. Emmerling, *J. Sol–Gel Sci. Technol.* **1998**, *13*, 299.
- [9] D. R. Rolison, B. Dunn, *J. Mater. Chem.* **2001**, *11*, 963.
- [10] A. C. Pierre, G. M. Pajonk, *Chem. Rev.* **2002**, *102*, 4243.
- [11] C. N. Chervin, B. J. Clapsaddle, H. W. Chiu, A. E. Gash, J. H. Satcher, Jr., S. M. Kauzlarich, *Chem. Mater.* **2005**, *17*, 3345.
- [12] C. Laberty-Robert, J. W. Long, E. M. Lucas, K. A. Pettigrew, R. M. Stroud, D. R. Rolison, *Chem. Mater.* **2006**, *18*, 50.
- [13] S. W. Tao, J. T. S. Irvine, *Ionics* **2000**, *6*, 389.
- [14] S. W. Tao, J. T. S. Irvine, *Mater. Res. Bull.* **2001**, *36*, 1245.
- [15] A. E. Gash, T. M. Tillotson, J. H. Satcher, Jr., J. F. Poco, L. W. Hrubesh, R. L. Simpson, *Chem. Mater.* **2001**, *13*, 999.
- [16] A. E. Gash, T. M. Tillotson, J. H. Satcher, Jr., L. W. Hrubesh, R. L. Simpson, *J. Non-Cryst. Solids* **2001**, *285*, 22.
- [17] A. E. Gash, J. H. Satcher, Jr., R. L. Simpson, *Chem. Mater.* **2003**, *15*, 3268.
- [18] J. W. Long, M. S. Logan, E. E. Carpenter, R. M. Stroud, D. R. Rolison, *J. Non-Cryst. Solids* **2004**, *350*, 182.
- [19] B. J. Clapsaddle, A. E. Gash, J. H. Satcher, Jr., R. L. Simpson, *J. Non-Cryst. Solids* **2003**, *331*, 190.
- [20] B. J. Clapsaddle, D. W. Sprehn, A. E. Gash, J. H. Satcher, Jr., R. L. Simpson, *J. Non-Cryst. Solids* **2004**, *350*, 173.
- [21] P. A. Webb, C. Orr, *Analytical Methods in Fine Particle Technology*. Micromeritics Instrument Corp., Norcross, GA **1997**.
- [22] J. W. Long, M. S. Logan, C. P. Rhodes, E. E. Carpenter, R. M. Stroud, D. R. Rolison, *J. Am. Chem. Soc.* **2004**, *126*, 16879.
- [23] J. Felsche, *Struct. Bonding (Berlin, Ger.)* **1973**, *13*, 99.
- [24] H. Okudera, Y. Masubuchi, S. Kikkawa, *Solid State Ionics* **2005**, *176*, 1473.
- [25] A. Emmerling, J. Gross, R. Gerlach, R. Goswin, G. Reichenauer, J. Fricke, H. G. Haubold, *J. Non-Cryst. Solids* **1990**, *125*, 230.
- [26] C. M. Parler, J. A. Ritter, M. D. Amiridis, *J. Non-Cryst. Solids* **2001**, *279*, 119.
- [27] A. Brisse, C. Barthet, A. L. Sauvet, S. Beaudet Savignat, J. Fouletier, in *Electrochem. Soc. Proc. PV2005-7*, The Electrochemical Society, Pennington, NJ **2005**, p. 363.
- [28] J. E. H. Sansom, D. Richings, P. R. Slater, *Solid State Ionics* **2001**, *139*, 205.
- [29] M. L. Anderson, C. A. Morris, R. M. Stroud, C. I. Merzbacher, D. R. Rolison, *Langmuir* **1999**, *15*, 674.
- [30] C. A. Morris, M. L. Anderson, R. M. Stroud, C. I. Merzbacher, D. R. Rolison, *Science* **1999**, *284*, 622.
- [31] J. J. Pietron, R. M. Stroud, D. R. Rolison, *Nano Lett.* **2002**, *2*, 545.
- [32] S. Célérier, *Ph.D. Thesis*, Université Paul Sabatier, Toulouse, France **2005**.